Localization-Centric OFDM Resource Allocation with Adaptive RIS Profiles in TN-NTN ISAC

Daniel Egea-Roca[1], Alda Xhafa[1], José A. del Peral-Rosado[2],
José A. López-Salcedo[1], and Gonzalo Seco-Granados[1]
[1] Dept. of Telecommunication and Systems Engineering, Universitat Autònoma de Barcelona
Centre d'Estudis i Recerca en Espai (CERES), IEEC, 08193 Bellaterra, Spain;
[2] Airbus Defence and Space, 82024 Taufkirchen, Germany

***Abstract*—This paper proposes a localization-centric Orthogonal Frequency Division Multiplexing (OFDM) resource-allocation framework for Reconfigurable Intelligent Surface (RIS)-assisted Terrestrial Network (TN)/Non-Terrestrial Network (NTN) Integrated sensing and communication (ISAC). The available OFDM subcarriers are partitioned into orthogonal TN and NTN combs, with NTN resources permanently dedicated to localization while the TN resources are dynamically allocated between localization and communication using a binary subcarrier mask. The proposed framework considers adaptive RIS configurations, with a random phase profile used during pre-feedback operation and a position-aware directional profile used after localization feedback. The subcarrier mask is optimized using a deterministic sequential-greedy search and evaluated in terms of the Multi-Layer Network (MuLa) Position Error Bound (PEB) and TN achievable rate. Numerical results show that the optimized allocation favors spectrally separated sensing resources and improves the localization–communication trade-off compared with a fixed 50/50 allocation. Furthermore, the directional RIS operation provides a substantial localization benefit over the random profile.**

***Index Terms*—ISAC, RIS, TN/NTN networks, OFDM resource allocation, localization, position error bound.**

I. Introduction

Accurate user localization is expected to become a fundamental capability of future 5G-Advanced and 6G networks, supporting not only positioning services but also communication functionalities such as environment-aware beamforming, mobility management, and interference coordination [1]. RIS-assisted networks rely on accurate user position information to configure directional phase profiles, making localization and communication tightly coupled rather than independent services. ISAC exploits this coupling by sharing spectrum, hardware, and waveforms between sensing and communication [1], [2]. RISs further enhance both functions by creating additional controllable propagation paths [3], [4], [5]. The integration of TN and NTN infrastructures combines the wide-area coverage of Low Earth Orbit (LEO) satellites with the high-capacity terrestrial links needed for RIS control signaling [6], [7].

Existing RIS-assisted ISAC research has focused on communication-oriented beamforming and RIS configurations to maximize spectral efficiency while supporting target sensing [5], [8]. Sensing-oriented work shows that passive RISs significantly improve radar detection and parameter estimation [9]. Localization-centric studies derive positioning bounds and estimators for RIS-aided systems, but typically assume fixed waveform resources and predefined communication allocations [4], [10]. Although OFDM resource allocation for positioning and communication has been studied without RIS [11], [12], extending it to RIS-assisted TN/NTN localization remains largely unexplored. In OFDM-based ISAC, the assignment of subcarriers between sensing and communication is a natural design variable: it controls which portion of the spectrum contributes to the localization Fisher Information Matrix (FIM) and which supports data transmission. When directional RIS beamforming is employed, this assignment is further constrained by the need to support the communication link for feeding back position estimates and RIS control parameters [13], tightening the coupling between localization and communication in the frequency domain.

Motivated by these observations, we optimize the binary TN sensing mask for fixed RIS operating profiles. All NTN subcarriers remain dedicated to localization, while communication uses the complementary TN subset. Random and directional RIS profiles represent pre- and post-feedback operation, respectively. The goal is to dynamically allocate subcarriers between sensing and communication through the binary mask, with the preference weight $\rho \in [0, 1]$, controlling the localization-communication trade-off. The contributions are threefold: (i) a localization-centric OFDM allocation evaluated through the MuLa PEB and temporal TN achievable rate; (ii) a deterministic sequential-greedy (SG) allocation with reduced-size exhaustive-search (ES) benchmarking; and (iii) characterization of the preference-weight trade-off, RIS operating condition, RIS–User Equipment (UE) distance, and TN/NTN layer contributions. Relative to our previous localization and RIS-profile studies [10], [7], [13], [14], the design variable here is the TN subcarrier mask in the ISAC framework rather than the RIS coefficients. Unlike the power-allocation and time-of-arrival formulations in [11], [12], we assume uniform per-layer power and optimize the multi-layer localization–communication trade-off using the PEB.

The rest of this paper is organized as follows. Section II in-

This work was supported by the Catalan government (New Space Strategy and AGAUR-ICREA Academia Program) and by AEI under grant PID2023-152820OB-I00 (MICIU/AEI/10.13039/501100011033, ERDF/EU).

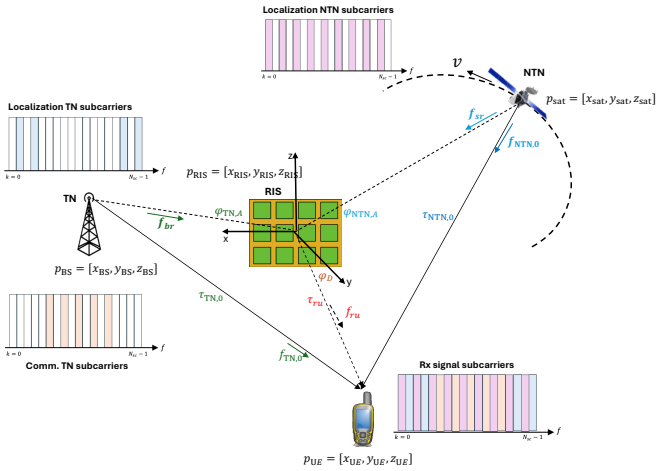


Fig. 1. System model of the proposed RIS-assisted MuLa ISAC framework. TN subcarriers are dynamically allocated to localization or communication, while NTN subcarriers are reserved for localization.

troduces the system model. Section III defines the performance metrics. Section IV formulates the proposed signal design and benchmark allocation. Section V presents numerical results, and Section VI concludes the paper.

II. RIS-Aided 5G/6G Localization-Centric ISAC

This section introduces the system model of the proposed RIS-assisted MuLa TN–NTN ISAC framework. A downlink ISAC scenario comprising one terrestrial base station (BS), one LEO satellite, one passive RIS, and one UE, where the RIS assists both the TN and NTN propagation paths is considered (see Fig. 1). Both transmitters employ OFDM with N_{sc} subcarriers, subcarrier spacing Δf, L OFDM symbols, and symbol duration $T_{\text{sym}} = T + T_{\text{CP}}$ with $T = 1/\Delta f$. The model assumes perfect TN and NTN synchronization, orthogonality between the two transmissions, and a common receiver clock bias Δt. The used model also accounts for the time-varying LEO trajectory and the resulting delay and Doppler evolution.

A. Channel Parameters

For layer $j \in \{\text{TN}, \text{NTN}\}$, and path $i \in \{0, 1\}$, with $i = 0$ and $i = 1$ denoting the direct and RIS-reflected paths, respectively, the channel parameters at symbol ℓ are the delay $\tau_{j,i}^{(l)}$, Doppler $f_{j,i}^{(l)}$, range rate $\nu_{j,i}^{(l)}$, and complex path gain $\alpha_{j,i}^{(l)}$; with $\ell = 0, \ldots, L-1$. For the NTN layer these quantities evolve with the LEO trajectory, with $\tau_{j,i}^{(\ell)} = r_{j,i}^{(\ell)}/c + \Delta t$ and $f_{j,i}^{(\ell)} = v_{j,i}^{(\ell)}/\lambda_j$, where $r_{j,i}^{(\ell)}$ is path length, $v_{j,i}^{(\ell)}$ is its range-rate coordinate, c is the speed of light, and $\lambda_j = c/f_{c,j}$ is the carrier wavelength with $f_{c,j}$ the carrier frequency. Collecting the L symbol-dependent delays and Dopplers in $\{\boldsymbol{\tau}_{j,i}, \boldsymbol{f}_{j,i}\} \in \mathbb{R}^{L\times 1}$, their effects are characterized with the $K_j \times L$ matrices $[\mathbf{D}(\boldsymbol{\tau}_{j,i}]_{k,l} = e^{-j2\pi\Delta_f k\tau_{j,i}^{(l)}}$, $[\mathbf{E}(\boldsymbol{f}_{j,i})]_{k,l} = e^{j2\pi f_{j,i}^{(l)}(kT/K)}$, and $[\mathbf{C}(\boldsymbol{f}_{j,i}))]_{k,l} = e^{j2\pi f_{j,i}^{(l)} l T_{\text{sym}}}$, while $\mathbf{A}_{j,i}$ contains the complex path gain including (free space) propagation loss and phase.

The RIS path additionally includes the RIS response, which is collected in $\mathbf{G}_{j,i}(\boldsymbol{\Phi}) \in \mathbb{C}^{K_j\times L}$, where $\boldsymbol{\Phi} = [\boldsymbol{\omega}_0, \ldots, \boldsymbol{\omega}_{L-1}] \in \mathbb{C}^{M\times L}$ contains the unit-modulus RIS coefficients. For the direct path $\mathbf{G}_{j,0}(\boldsymbol{\Phi}) \equiv \mathbf{1}$, whereas

$$[\mathbf{G}_{j,1}(\boldsymbol{\Phi})]_{:,l} = \left[\mathbf{a}_j\left(\phi_A^{(j)}, \theta_A^{(j)}\right) \odot \mathbf{a}_j\left(\phi_D, \theta_D\right)\right]^\top \boldsymbol{\omega}_l. \tag{1}$$

Here, $\mathbf{a}_j(\cdot) \in \mathbb{C}^{M\times 1}$ is the RIS steering vector at λ_j; the Angle of Arrival (AoA) is known and (ϕ_D, θ_D) denotes the RIS–UE departure direction. A common physical RIS configuration is assumed for both layers, with far-field and narrowband responses. Random and position-aware directional profiles [13] are considered in this paper for the pre- and post-feedback operating conditions, respectively.

B. Signal Model

Let $\mathcal{K} = \{1, \ldots, N_{sc}\}$ denote the active OFDM subcarrier set. The TN and NTN layers occupy two disjoint interleaved subcarrier combs, $\mathcal{K} = \mathcal{K}_{\text{TN}} \dot\cup \mathcal{K}_{\text{NTN}}, \mathcal{K}_{\text{TN}} \cap \mathcal{K}_{\text{NTN}} = \varnothing$. The combs describe layer-specific baseband resources at distinct (layer) carrier frequencies, with even indices assigned to TN and odd indices assigned to NTN. The terrestrial comb is further partitioned into sensing and communication subsets, $\mathcal{K}_{\text{TN}} = \mathcal{K}_{\text{s}} \dot\cup \mathcal{K}_{\text{c}}, \mathcal{K}_{\text{s}} \cap \mathcal{K}_{\text{c}} = \varnothing$, where $\mathcal{K}_{\text{s}}$ contains the TN subcarriers used for localization sensing and $\mathcal{K}_{\text{c}}$ those used for communication. The terrestrial allocation is encoded by the binary sensing mask

$$[\mathbf{m}]_k = m_k = \begin{cases} 1, & k \in \mathcal{K}_{\text{s}}, \\ 0, & k \in \mathcal{K}_{\text{c}}, \end{cases} \qquad k \in \mathcal{K}_{\text{TN}}. \tag{2}$$

Each transmitter sends pilot symbols $x_{k,l}^{(j)}$ over its assigned sensing-subcarrier set $\mathcal{K}_j$, while TN transmitter additionally sends data symbols $x_{k,l}^{\text{TN}}$ over $k \in \mathcal{K}_{\text{c}}$.

Following [14], the received signal for layer j and propagation path i, collected over K_j active subcarriers and during L OFDM symbols, is

$$\begin{aligned} \mathbf{Y}_{j,i} &= \mathbf{A}_{j,i} \odot \mathbf{F}_j\left(\mathbf{E}(\mathbf{f}_{j,i}) \odot \mathbf{F}_j^H \mathbf{Z}_{j,i}\right), \\ \mathbf{Z}_{j,i} &= \mathbf{C}(\mathbf{f}_{j,i}) \odot \mathbf{D}(\boldsymbol{\tau}_{j,i}) \odot \mathbf{G}_{j,i}(\boldsymbol{\Phi}) \odot \mathbf{X}_j. \end{aligned} \tag{3}$$

where $\mathbf{F_j}$ is the unitary $K_j \times K_j$ Discrete Fourier Transform (DFT) matrix, $\mathbf{X}_j$ contains the transmitted OFDM symbols, and the remaining factors defined in Section II-A.

The total MuLa observation, with each layer matrix embedded in its assigned resources, is

$$\mathbf{Y} = \sum_{j\in\{\text{TN},\text{NTN}\}} (\mathbf{Y}_{j,0} + \mathbf{Y}_{j,1}) + \mathbf{W}, \tag{4}$$

where $\mathbf{W}$ is complex additive white Gaussian noise (AWGN). For a communication subcarrier $k \in \mathcal{K}_{\text{c}}$, the scalar frequency-domain observation at symbol l reduces to

$$Y_{k,l} = H_{k,l}(\boldsymbol{\Phi})\, x_{k,l}^{(\text{TN})} + W_{k,l}, \tag{5}$$

where the effective channel coefficient decomposes as

$$H_{k,\ell}(\Phi) = H_{d,k} + H_{r,k}^{(\ell)}(\Phi), \tag{6}$$

into the direct BS–UE contribution $H_{d,k}$ and the RIS-reflected component $H_{r,k}^{(l)}(\boldsymbol{\Phi})$, the latter controlled by (1). This decomposition directly supports the capacity metric derived in Section III.

C. Localization-Centric Sensing Stage

Localization uses the TN sensing subset $\mathcal{K}_{\mathrm{s}}$ and the complete NTN subset $\mathcal{K}_{\mathrm{NTN}}$. Hence, the sensing mask modifies only the terrestrial localization information, whereas the NTN contribution remains fixed. Two RIS phase configurations are used throughout this work: Random RIS represents initial pre-feedback operation, and directional RIS represents position-aware post-feedback operation. During each optimization run, the selected RIS phase profile is kept fixed.

For localization, we process the channel parameters estimated during the sensing stage to extract the UE position and clock bias. The channel parameters include information we want to estimate for each layer j and path i, such as propagation delays $\boldsymbol{\tau} \in \mathbb{R}^4$ and angular measures $\boldsymbol{\vartheta} \in \mathbb{R}^4$. These parameters are collected into the desired parameter vector $\boldsymbol{\theta} = [\boldsymbol{\tau}^\top \boldsymbol{\vartheta}^\top]^\top$. Furthermore, we have aditional nuisance parameters that must be estimated to get a correct estimation of the desired parameters. These are the per-layer and per-path Doppler-related range-rate parameters $\mathbf{v} \in \mathbb{R}^4$, and complex channel gains $\boldsymbol{\alpha} \in \mathbb{C}^4$. This gives the channel parameter vector

$$\boldsymbol{\gamma} = \left[\boldsymbol{\tau}^T, \boldsymbol{\vartheta}^T, \mathbf{v}^T, \Re\{\boldsymbol{\alpha}\}^T, \Im\{\boldsymbol{\alpha}\}^T\right]^T = \left[\boldsymbol{\theta}^\top, \boldsymbol{\zeta}^\top\right]^\top, \quad (7)$$

with $\boldsymbol{\zeta} \in \mathbb{R}^{12}$ the nuisance parameters.

Channel parameter estimation is possible due to the opposite signs of the RIS profile used on consecutive OFDM symbols, $\boldsymbol{\omega}_{2p-1} = -\boldsymbol{\omega}_{2p-2}$, $p = 1, \ldots, L/2$; enabling direct/RIS path separation through sum/difference processing [4]. Together with known BS, RIS, and satellite states, the channel parameters provide information about the measure of interest

$$\boldsymbol{\eta} = [\mathbf{p}^\top, \boldsymbol{\zeta}^\top]^\top, \quad (8)$$

where $\mathbf{p} = [p_x, p_y, p_z, \Delta t]^\top$ includes the position-domain state vector with the UE position and clock bias. In the initial sensing stage, a random RIS profile provides a UE-position estimate. This estimate can subsequently be fed back to the network to configure the position-aware directional profile.

D. Communication Stage

The communication stage uses only the TN communication subset $\mathcal{K}_{\mathrm{c}}$, while NTN layer is dedicated to localization and therefore not included in the communication-capacity metric. For each consecutive RIS-sign pair p, the two effective channels are

$$H^{+}_{k,p} = H_{d,k} + H^{(p)}_{r,k}(\boldsymbol{\Phi}), \qquad H^{-}_{k,p} = H_{d,k} - H^{(p)}_{r,k}(\boldsymbol{\Phi}), \quad (9)$$

where $H^{(p)}_{r,k}$ is the reflected contribution before the paired sign. Capacity is obtained by evaluating the averaged rate among each (pair) state. In the proposed localization-feedback framework, this stage represents post-feedback operation: the estimated UE position is conveyed through the TN link and used to configure the directional RIS profile. Feedback latency, errors and closed-loop protocol implementation are outside the scope of this work.

III. ISAC Performance Bounds

This section defines the performance metrics used to optimize the proposed localization-centric ISAC framework. The binary sensing mask $\mathbf{m}$ determines the sensing and communication resource allocation, thereby defining the localization-communication trade-off. Specifically, the sensing metric captures delay/frequency diversity, the communication metric captures the TN communication capacity metric, and the localization metric is given by MuLa PEB.

A. Localization Bounds

The localization performance is characterized by the MuLa PEB. For each layer j, the channel-domain FIM [15] associated with $\boldsymbol{\gamma}_j \in \mathbb{R}^{10}$ is

$$\left[\mathbf{J}^{(j)}_{\gamma}\right]_{r,c} = \frac{2P_{s,j}}{\sigma^2} \Re\left\{ \sum_{\ell=0}^{L-1} \sum_{k \in \mathcal{K}^{\mathrm{loc}}_j} \frac{\partial M^{(j)}_{k,\ell}}{\partial \gamma_{j,r}} \left(\frac{\partial M^{(j)}_{k,\ell}}{\partial \gamma_{j,c}} \right)^H \right\}, \quad (10)$$

where $P_{s,j} = P_j/|\mathcal{K}_j|$, $\mathcal{K}^{\mathrm{loc}}_{\mathrm{TN}} = \mathcal{K}_s$, $\mathcal{K}^{\mathrm{loc}}_{\mathrm{NTN}} = \mathcal{K}_{\mathrm{NTN}}$, and $M^{(j)}_{k,\ell}$ denotes the noiseless observation in (3). The orthogonal TN/NTN contributions are mapped to the common position-domain state through the corresponding geometry Jacobian $\mathbf{T}_j = \partial \boldsymbol{\gamma}_j / \partial \boldsymbol{\eta}^\top$ as

$$\mathbf{J}_{\eta} = \sum_{j \in \{\mathrm{TN}, \mathrm{NTN}\}} \mathbf{T}_j^T \mathbf{J}^{(j)}_{\gamma} \mathbf{T}_j. \quad (11)$$

Partitioning $\mathbf{J}_\eta$ into the position/clock ($\mathbf{J}_p$) and nuisance blocks ($\mathbf{J}_\zeta$), the EFIM $\mathbf{J}_{\mathrm{e}} \in \mathbb{R}^4$ is

$$\mathbf{J}_{\mathrm{e}} = \mathbf{J}_p - \mathbf{J}_{p\zeta} \mathbf{J}_{\zeta}^{-1} \mathbf{J}_{\zeta p}, \quad (12)$$

where the cross-terms correspond to the off-diagonal blocks in the FIM. The corresponding MuLa PEB is

$$\mathrm{PEB}(\mathbf{m}; \boldsymbol{\Phi}) = \sqrt{\mathrm{tr}\left(\left[(\mathbf{J}_{\mathrm{e}}^{-1}\right]_{1:3,1:3}\right)}. \quad (13)$$

Although the PEB depends jointly on geometry and channel parameters, the delay-information contribution satisfies

$$J_\tau \propto |\mathcal{K}_s| \beta^2_{\mathrm{rms}},$$

so increasing the sensing bandwidth or selecting spectrally separated subcarriers toward the band edges improves delay information [16], [17], at the expense of communication resources. This relation explains the allocation structure, while the optimization is ultimately evaluated using the MuLa PEB in Section IV.

B. Communication Bounds

For a fixed sensing mask, the terrestrial communication capacity averages the capacity of each (symbol) state over $P = L/2$ RIS sign pairs. For even L we get

$$C(\mathbf{m}; \Phi) = \sum_{k \in \mathcal{K}_{\mathrm{c}}} \frac{\Delta f}{2P} \sum_{p=1}^{P} \left[\log_2(1 + \gamma^{+}_{k,p}) + \log_2(1 + \gamma^{-}_{k,p})\right], \quad (14)$$

$$\gamma^{\pm}_{k,p}(\Phi) = \frac{P_{s,\mathrm{TN}} |H^{\pm}_{k,p}(\Phi)|^2}{\sigma^2}.$$

Here $P_{s,\mathrm{TN}} = P_{\mathrm{TN}}/|\mathcal{K}_{\mathrm{TN}}|[\mathrm{W}]$ is the transmit power per active TN subcarrier, and $\sigma^2 = N_0\Delta f$ is the noise power per subcarrier. Moreover, the $N_0 = k_B T_{\mathrm{noise}} F[\mathrm{W/Hz}]$ denotes the effective receiver noise power spectral density, where $k_B = 1.380649\times10-23\mathrm{J/K}$ is the Boltzmann constant, T_{noise} is the noise temperature, and $F = 10^{NF/10}$ is the linear noise factor, with NF denoting the noise figure in dB.

Each logarithm in (14) is evaluated for one RIS (symbol) state; averaging over both states and all P pairs accounts for their temporal occurrence. The outer sum combines TN communication-carrier rates, giving capacity in bit/s. We consider uniform power among all carriers, thus power is not included in the allocation mask. Note that the sum in (14) is evaluated only over TN communication subcarriers $\mathcal{K}_{\mathrm{c}}$, while sensing subcarriers contribute to localization but not to the communication metric. Similarly, NTN is used only for sensing, so that it does not contribute capacity to this architecture.

IV. Localization-Centric OFDM Signal Design

This section proposes a localization-centric OFDM signal design for the considered RIS-aided MuLa ISAC system. The design variable is the binary TN sensing mask $\mathbf{m}$, which determines whether each terrestrial subcarrier is assigned to sensing or communication. The remaining parameters are classified as inputs and constraints. Input parameters are assumed to be given, including the OFDM grid, the BS-RIS-UE geometry, the transmit powers, the noise level, and the fixed TN/NTN subcarrier partition. The constraint parameters include the selected RIS phase profile and the minimum sensing and communication resource requirements. Throughout optimization, the NTN allocation and the RIS phase profile remain fixed. Based on this framework, we first formulate the constrained signal design problem, then define the ISAC optimization criterion, and finally describe the optimization algorithm.

A. ISAC Performance Optimization

For a fixed RIS profile $\mathbf{\Phi}$, the optimization is controlled by a preference weight $\rho \in [0,1]$, which selects the desired operating point along the localization-communication trade-off. The feasible set is defined by minimum sensing and communication allocation resource requirements. Thus, the following constraints are defined: C1 : $|\mathcal{K}_{\mathrm{s}}(\mathbf{m})| \geq K_{\mathrm{s}}^{\min}$ and C2 : $|\mathcal{K}_{\mathrm{c}}(\mathbf{m})| \geq K_{\mathrm{c}}^{\min}$. These constraints prevent degenerate sensing-only or communication-only designs and keep both ISAC functions active on the TN comb. Furthermore, we maintain uniform power allocation among the sensing/communication subcarriers of the TN layer with C3 : $[\mathbf{m}]_k = m_k \in \{0,1\},\ k \in \mathcal{K}_{\mathrm{TN}}$. The normalized ISAC objective is

$$J_\rho(\mathbf{m};\mathbf{\Phi}) = \rho\frac{\mathrm{PEB}(\mathbf{m};\mathbf{\Phi})}{\mathrm{PEB}_{\mathrm{ref}}(\mathbf{\Phi})} + (1-\rho)\frac{C_{\max}(\mathbf{\Phi})}{C(\mathbf{m};\mathbf{\Phi})}, \qquad (15)$$

where the first term promotes localization accuracy through the MuLa PEB in (13), and the second promotes communication throughput through the TN capacity in (14).

The fixed normalization references are computed separately for each RIS profile. $\mathrm{PEB}_{\mathrm{ref}}$ uses a mask reserving the $K_c^{\min}$ TN subcarriers closest to band center for communication; it is a reference value, not a demonstrated global PEB optimum. $C_{\max}$ reserves the $K_s^{\min}$ subcarriers with the smallest rate contributions for sensing. The constrained design problem is defined by

$$\mathbf{m}^\star(\rho;\mathbf{\Phi}) = \arg\min_{\mathbf{m}} \quad J_\rho(\mathbf{m};\mathbf{\Phi}) \quad \text{s.t. C1} - \text{C3}. \qquad (16)$$

For every value of ρ and every selected RIS profile, the optimization returns one binary sensing mask $\mathbf{m}^\star$. Setting $\rho = 1$ gives a localization-centric allocation, $\rho = 0$ gives a communication-centric allocation, and intermediate values select scalarized preference points. Sweeping ρ provides a mechanism for selecting the operating point according to the desired positioning and communication requirements. Note that because the mask-dependent terms are nonlinear, uniformly spaced weights do not necessarily yield uniformly spaced operating points in the PEB–capacity plane.

B. Sequential Greedy Optimization

The optimization problem in (16) is combinatorial, since the search space consists of all feasible binary sensing masks and therefore grows exponentially with the number of TN subcarriers. To obtain practical solutions, we employ deterministic sequential greedy (SG). It starts from the minimum feasible sensing allocation and progressively adds one sensing subcarrier at a time. At each stage, all feasible one-subcarrier additions are evaluated using the objective in (15), including MuLa PEB and TN capacity over all configured symbols. The candidate yielding the lowest objective is selected, producing a nested sequence of masks spanning all feasible sensing cardinalities. SG returns the mask with the lowest objective among those evaluated along this sequence. In the considered scenario, the two TN band-edge subcarriers initialize the sensing allocation. The resulting SG search scales quadratically with the number of TN subcarriers, whereas exhaustive search (ES) grows combinatorially and is therefore used only as an optimality benchmark for a reduced-size problem.

Frequency allocation is optimized independently for each fixed RIS profile. Random RIS represents the pre-feedback operation and the directional RIS position-aware post-feedback operation. A fixed interleaved 50/50 allocation with random RIS provides a reference for adaptive resource allocation. RIS profile affects both the communication channel and the localization information, thus, SG evaluates the complete objective for each profile rather than optimizing RIS coefficients jointly with the mask.

V. Numerical Results

This section evaluates the proposed localization-centric OFDM resource-allocation framework using the Frequency Range 1 (FR1) setup in Table I. The considered scenario follows Fig. 1 and includes a passive RIS, independent TN/NTN power budgets, thermal noise with receiver noise figure, and a single-LEO trajectory. Two RIS phase profiles are

TABLE I
DEFAULT FR1 SIMULATION PARAMETERS.

Parameter	Value
Carrier freq. TN / NTN	2.13 / 2.185 GHz
Subcarriers N_{sc}	288 (144 TN, 144 NTN)
Subcarrier spacing Δf	30 kHz
OFDM symbols L	288
TN / NTN tx power	23 / 53 dBm
Noise temp. / NF	290 K / 8 dB
BS position	$(15, 10, 5)$ m
RIS position	$(0, 0, 0)$ m
UE position	$(20, -20, -1.5)$ m
LEO altitude / elevation	1200 km / 45°
LEO inclination	53°
LEO orbit	Circular
RIS Array size	16×16 (256 elements)
RIS Element spacing	$0.5\lambda_{\mathrm{TN}} = 0.0704$ m
RIS Phase profiles	Random and directional
RIS Temporal modulation	Alternating sign
ρ sweep	$\{0, 0.1, \ldots, 1\}$
Constraints	$K_s^{\min}$=2, $K_c^{\min}$=1

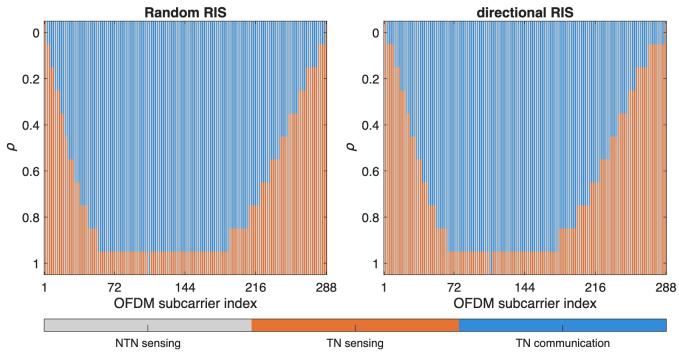


Fig. 2. Optimized carrier-allocation masks for random and directional RIS profiles. Each row corresponds to a different ρ. Colors denote corresponding subcarrier allocations.

considered: random and directional. Unless otherwise stated, the UE remains at the reference position in Table I. Throughout the optimization, all NTN subcarriers remain assigned to localization, while only the TN allocation is optimized. Performance is evaluated in terms of the MuLa PEB and the TN communication capacity in (14).

A. Frequency Allocation

The first analysis investigates how the optimizer distributes the TN OFDM subcarriers as the preference weight ρ varies. Small values of ρ prioritize communication, whereas larger values progressively favor localization. The performance is compared for random and directional RIS profiles, together with a fixed 50/50 interleaved allocation used as a benchmark. Fig. 2 illustrates the optimized allocation masks. For low ρ, only the minimum number of TN subcarriers is assigned to sensing, while most of the band is reserved for communication. As ρ increases, more sensing resources are selected with a preference for band-edge carriers, leaving the central frequencies mainly for communication. At $\rho = 1$, nearly all TN subcarriers are devoted to sensing, with minimum communication allocation retained. The preference for separated edge carriers relates to their effective sensing bandwidth and delay information. The full PEB additionally depends on geometry, channel conditions and RIS profile. The allocation counts in Fig. 3 show that the profiles can lead to different TN resource

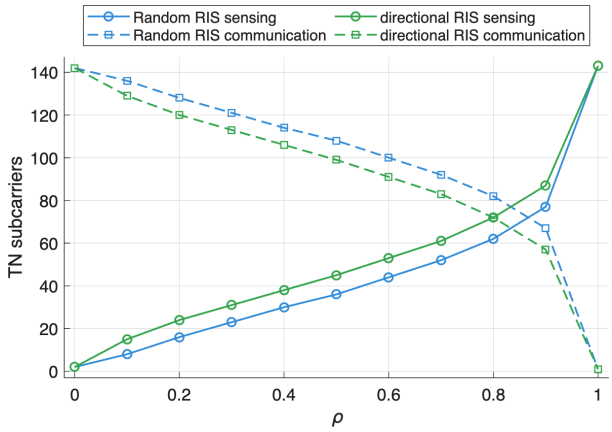


Fig. 3. Number of TN sensing and communication subcarriers versus ρ for random and directional RIS profiles.

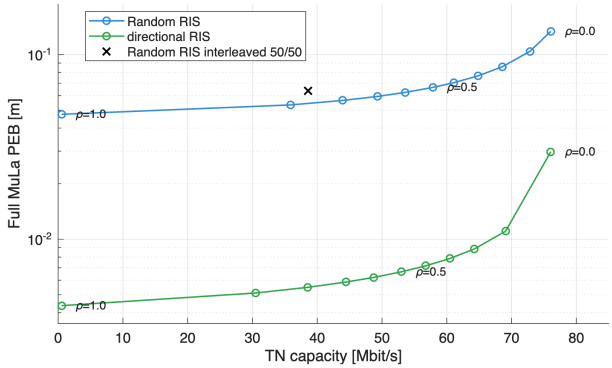


Fig. 4. MuLa PEB-capacity operating points across the ρ sweep for random and directional RIS profiles. The random-RIS interleaved 50/50 allocation is included as a benchmark reference.

splits. At $\rho = 0.5$, Random RIS assigns 36 sensing and 108 communication carriers, whereas directional RIS assigns 45 and 99, respectively. Increasing ρ favors localization, but neither carrier counts nor physical performance vary linearly with this preference weight.

B. Localization–Communication Performance

The second analysis evaluates the localization–communication trade-off achieved by the optimized allocation. Fig. 4 shows the resulting discrete PEB–capacity operating points obtained by sweeping ρ. At $\rho = 0.5$, Random RIS gives a PEB of 6.64 cm and capacity of 57.85 Mbit/s; directional RIS gives 0.67 cm and 53.00 Mbit/s. Directional RIS provides lower nominal PEB, while its independently selected allocation uses more sensing carriers at this weight. A general capacity gain is not implied. The Random RIS interleaved 50/50 reference illustrates a fixed allocation; minimizing the scalar objective in this case does not mean independently maximizing both metrics. Sweeping ρ gives the signal designer a mechanism to move among operating points according to the application requirements and the propagation conditions.

To examine geometry and MuLa information, the UE is moved along the diagonal direction $[+x, -y]$ from the RIS preserving the nominal UE height and fixing $\rho = 0.5$. Fig. 5

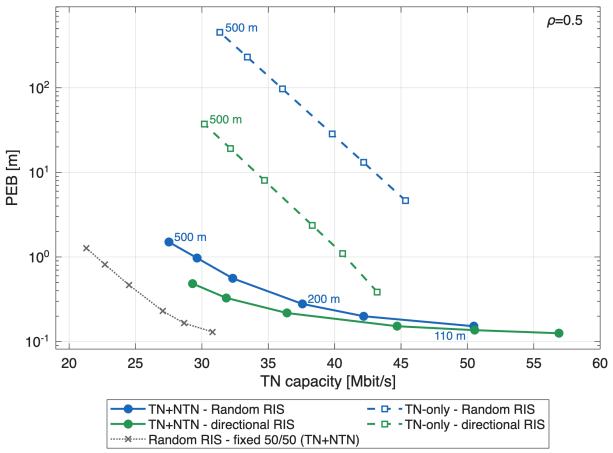


Fig. 5. MuLa PEB and TN capacity versus RIS-UE distance for $\rho = 0.5$. Optimized random and directional RIS allocations versus the interleaved 50/50 benchmark.

compares independently SG-optimized TN+NTN and TN-only allocations for both RIS profiles at different distances. The MuLa improvement relative to TN increases monotonically over the simulated $110 - 500$ m range for both profiles. This MuLa benefit reflects complementary TN and NTN information combined in the common position-domain FIM before nuisance elimination. NTN becomes increasingly valuable as terrestrial-only localization weakens. Geometry also changes capacity and the preferred resource split: at 500 m, TN+NTN uses $51/93$ sensing/communication carriers under Random RIS and $45/99$ under directional RIS, whereas independently optimized TN-only uses $38/106$ and $42/102$, respectively.

As a computational benchmark, for a reduced problem with 16 TN subcarriers, SG recovered the ES optimum and identical allocation mask in all six tested cases. SG required 105 objective evaluations versus 65518 for ES ($\approx 624\times$ fewer), with runtimes of 2.5–2.9 s and 257–260 s, respectively.

VI. Conclusions

This work shows that localization-centric TN resource allocation can effectively manage the positioning–communication trade-off in RIS-assisted TN/NTN ISAC. The optimized masks consistently favor spectrally separated sensing carriers while preserving the remaining TN resources for communication, outperforming the fixed 50/50 allocation benchmark. Position-aware directional RIS operation substantially improves localization relative to the random pre-feedback condition, although the corresponding communication gain depends on the selected operating point. The distance analysis further shows that the NTN contribution becomes increasingly relevant as terrestrial-only localization degrades, highlighting the value of multi-layer information fusion beyond short-range scenarios with favorable TN geometry. Finally, SG reproduces the exhaustive-search optimum in the reduced benchmark with substantially lower complexity, supporting its use for the full-size problem. Overall, the results demostrate that adaptive TN allocation and position-aware RIS control provide complementary mechanisms for selecting application-dependent localization–communication operating points.

References

[1] F. Liu, Y. Cui, C. Masouros, J. Xu, T. X. Han, Y. C. Eldar, and S. Buzzi, "Integrated sensing and communications: Toward dual-functional wireless networks for 6g and beyond," *IEEE journal on selected areas in communications*, vol. 40, no. 6, pp. 1728–1767, 2022.

[2] C. Masouros, J. A. Zhang, F. Liu, L. Zheng, H. Wymeersch, and M. Di Renzo, "Guest editorial: Integrated sensing and communications for 6g," *IEEE Wireless Communications*, vol. 30, no. 1, pp. 14–15, 2023.

[3] M. Di Renzo, A. Zappone, M. Debbah, M.-S. Alouini, C. Yuen, J. De Rosny, and S. Tretyakov, "Smart radio environments empowered by reconfigurable intelligent surfaces: How it works, state of research, and the road ahead," *IEEE journal on selected areas in communications*, vol. 38, no. 11, pp. 2450–2525, 2020.

[4] K. Keykhosravi, M. F. Keskin, G. Seco-Granados, P. Popovski, and H. Wymeersch, "RIS-enabled SISO localization under user mobility and spatial-wideband effects," *IEEE Journal of Selected Topics in Signal Processing*, vol. 16, no. 5, pp. 1125–1140, 2022.

[5] D. Kompostiotis, D. Vordonis, K. D. Katsanos, F.-C. Grec, V. Paliouras, and G. C. Alexandropoulos, "Ris-aided localization and sensing," *arXiv preprint arXiv:2512.00205*, 2025.

[6] S. Saleh, P. Zheng, X. Liu, H. Chen, M. F. Keskin, B. Priyanto, M. Beale, Y. Ettefagh, G. Seco-Granados, T. Y. Al-Naffouri *et al.*, "Integrated 6g tn and ntn localization: Challenges, opportunities, and advancements," *IEEE Communications Standards Magazine*, 2025.

[7] A. Xhafa, D. Egea-Roca, J. A. Lopez-Salcedo, and G. Seco-Granados, "A Comparative analysis of key performance indicators for RIS-enhanced non-terrestrial and terrestrial localization," in *Proc. European Signal Processing Conference (EUSIPCO)*, Sep. 2025.

[8] R. Du, Z. Wei, Z. Yang, Y.-F. Liu, B. Zhou, and D. W. K. Ng, "Ofdm waveform optimization for bistatic integrated sensing and communications," *arXiv preprint arXiv:2603.08442*, 2026.

[9] S. Buzzi, E. Grossi, M. Lops, and L. Venturino, "Radar target detection aided by reconfigurable intelligent surfaces," *IEEE Signal Processing Letters*, vol. 28, pp. 1315–1319, 2021.

[10] D. Egea-Roca, A. Xhafa, J. A. Lopez-Salcedo, and G. Seco-Granados, "Performance assessment of multi-RIS-aided localization in terrestrial and non-terrestrial networks," in *Proc. European Navigation Conference (ENC)*, May 2025.

[11] R. Montalban, J. A. López-Salcedo, G. Seco-Granados, and A. L. Swindlehurst, "Power allocation approaches for combined positioning and communications ofdm systems," in *2013 IEEE 14th Workshop on Signal Processing Advances in Wireless Communications (SPAWC)*. IEEE, 2013, pp. 694–698.

[12] A. M. Graff and T. E. Humphreys, "Ziv-zakai-optimal ofdm resource allocation for time-of-arrival estimation," *IEEE Transactions on Wireless Communications*, 2025.

[13] A. Xhafa, D. Egea-Roca, J. A. Lopez-Salcedo, S. Schlötzer, J. A. del Peral-Rosado, F. Abel, and G. Seco-Granados, "Hybrid random-directional ris phase profile design for multi-layer tn/ntn positioning," in *Proc. ESA Workshop on Satellite Navigation User Equipment Technologies (NAVITEC)*, May 2026.

[14] D. Egea-Roca, A. Xhafa, J. A. López-Salcedo, and G. Seco-Granados, "First results on ris-enabled multi-layer localization: A joint terrestrial and non-terrestrial method," in *2026 IEEE International Conference on Acoustics, Speech, and Signal Processing*. IEEE, 2026.

[15] S. M. Kay, *Fundamentals of Statistical Signal Processing: Estimation Theory*. Upper Saddle River, NJ, USA: Prentice Hall, 1993, vol. 1.

[16] A. Liu, Z. Huang, M. Li, Y. Wan, W. Li, T. X. Han, C. Liu, R. Du, D. K. P. Tan, J. Lu *et al.*, "A survey on fundamental limits of integrated sensing and communication," *IEEE Communications Surveys & Tutorials*, vol. 24, no. 2, pp. 994–1034, 2022.

[17] J. A. del Peral-Rosado, J. A. López-Salcedo, G. Seco-Granados, F. Zanier, and M. Crisci, "Achievable localization accuracy of the positioning reference signal of 3gpp lte," in *2012 international conference on localization and GNSS*. IEEE, 2012, pp. 1–6.